IEEE Access
Multidisciplinary | Rapid Review | Open Access Journal

Received September 10, 2019, accepted September 23, 2019, date of publication September 27, 2019,
date of current version October 9, 2019.

Digital Object Identifier 10.1109/ACCESS.2019.2944206

Optimal Design of a Nonlinear Series Elastic Actuator for the Prosthetic Knee Joint Based on the Conjugate Cylindrical Cam

YUANXI SUN[1], PEI TANG[1], JIA ZHENG[2], DIANBIAO DONG[3,4], XIAOHONG CHEN[1], LONG BAI[1], AND WENJIE GE[3]

[1]State Key Laboratory of Mechanical Transmission, Chongqing University, Chongqing 400044, China
[2]School of Advanced Manufacturing Engineering, Chongqing University of Posts and Telecommunications, Chongqing 400065, China
[3]School of Mechanical Engineering, Northwestern Polytechnical University, Xi'an 710072, China
[4]Department of Mechanical Engineering, Vrije Universiteit Brussel, 1050 Brussels, Belgium

Corresponding author: Yuanxi Sun (sunyuanxi@ cqu.edu.cn)

This work was supported in part by the Fundamental Research Funds for the Central Universities under Grant 2018CDXYJX0019 and Grant 2019CDCGJX219, and in part by the National Natural Science Foundation of China under Grant 51975070.

ABSTRACT Active actuation is an essential method to enhance the performance of the prosthetic knee joint. In this paper, a new nonlinear series elastic actuator based on the conjugate cylindrical cam (N3CSEA) is proposed for the actuation of the prosthetic knee in level-ground walking. The N3CSEA, which is optimized with multi-objective of reducing its actuation power and enhancing its mechanical properties, uses two conjugate cylindrical cams to nonlinearly actuate their corresponding helical springs, thus generating required output torques for the prosthetic knee. Unlike conventional SEAs, the motor of the N3CSEA rotates unidirectionally, and its rotation speed is linearly related to the walking speed of the prosthetic knee, thereby reducing the total electric energy consumption of the motor as well as the difficulty of motor control. In addition, the first cam system in the N3CSEA is set responsible for the stance actuation and the second one is set for the swing actuation, which can realize seamless switching of stance and swing in level-ground walking. An N3CSEA-integrated prosthetic knee joint is built for verification, and the experiment shows that the N3CSEA-actuated prosthetic knee joint is of high electric power efficiency.

INDEX TERMS Conjugate cylindrical cam, nonlinear series elastic actuator, prosthetic knee joint.

I. INTRODUCTION

With the rapid development of prosthetic technology, the actuation has become a critical factor that restricts the practicality of the prosthetic knee joint. Many efforts are made to improve the performance of the prosthetic actuation, among which the series elastics actuators (SEA) are the most successful and widely applied devices [1]–[5]. The SEA uses the controllable deformation of the series spring to achieve precise outputs of the force/torque, thus providing better control accuracy and stability, as well as better shock tolerance than the direct actuation of the motor. In addition, the spring in the SEA can store released energy from the load during periodic motion, thereby enhancing the overall energy efficiency of actuation [6], [7].

The associate editor coordinating the review of this manuscript and approving it for publication was Aysegul Ucar.

The SEAs commonly implemented in the prosthetic joints use helical springs and linear transmission devices such as screws, gears, and pulleys to achieve compliant actuation. For example, Au et al. proposed a powered ankle prosthesis actuated by the SEA and a unidirectional parallel spring [8], which can lower the metabolic cost of walking in amputees [9]. Lagoda et al. designed a direct-mounted electric SEA [10] capable of providing sufficient torque for robotic gait rehabilitation training at average walking speed. Paine and Sentis et al. presented a compact prismatic SEA integrated with a pushrod that allows the actuator to be installed within the robotic leg [11], [12]. To reduce the weight and provide adjustable torque for the joint, Veneman *et al*. used the Bowden cable-driven SEA to actuate an exoskeleton-type rehabilitation robot [13].

In addition to helical springs, spiral springs are also widely applied in SEAs due to their advantages of compact size and

more design parameters than the helical spring. For example, Zhang and Huang developed a compact SEA unit by a flat motor, a harmonic transmission, and a flat torsional spring, which is of small axial dimension in the application of the hip exoskeleton [14], [15]. Accoto and Carpino et al. designed a SEA with a novel architecture to output 300W for the lower limb robotic orthosis, in which the spiral spring is optimized to achieve a low intrinsic stiffness with minimum weight and dimensions [16], [17]. Moreover, Kim et al. proposed a dual-spiral-spring actuation system, which can achieve higher levels of compliance and deformation compared with other elastic components [18].

Some researchers took advantage of different drive components or add additional mechanisms to improve the actuation performance of SEAs. For example, Ates et al. used RC servos to develop a miniature SEA for the hand orthosis [19], and Zheng et al. proposed a pneumatic SEA capable of supporting a 75kg individual [20], [21]. In addition, Garcia et al. combined the SEA with the magneto-rheological damper to achieve a 20% reduction in the energy wasted in braking the knee during its extension in the leg stance phase [22], and Rouse et al. developed a clutchable SEA which can reduce the overall energy consumption of the actuator [23], [24].

The aforementioned SEAs differ in shapes and structures. However, they are essentially the linear SEA, i.e., the connection relationship between the motor and the load is linear transmission/spring, which can be described by the model shown in Fig. 1.

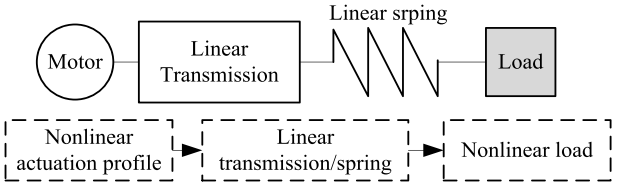

FIGURE 1. Model of the linear SEA.

Although the linear SEA performs well in various applications of robotics, prosthesis, and exoskeletons, etc., there are two unintentionally neglected issues:

(1) Major issue: high motor electric power consumption/low motor electric power efficiency: in applications with the nonlinear load (i.e., the relationship between the velocity and torque profile is nonlinear), the motor in the linear SEA must output required nonlinear motion. When the motor runs under non-nominal conditions, for example, the situation of high torque and low speed, the Joule losses in the motor will increase dramatically, thereby decreasing the electric power efficiency. Although in large-size applications such as electric cars or trains, multi-stage linear transmissions can be applied to make the motor run near its max efficiency state, it is not easy to realize miniature multi-stage transmissions for wearable devices or miniaturized robotics. In addition, inertial torques (caused by the moment of inertia of the transmission and the motor rotor) in the system may also increase the electric power of the motor, resulting in the extra energy loss for the whole actuation system. when motor controllers of electrical energy regeneration functions are used, the inertial energy loss can be neglected in periodic motions [25]. However, rapid changes in motor rotation directions will still increase the instantaneous electric power of the motor, which may have some negative impact on the peak power of the motor. Moreover, when using common motor controllers, which cannot generate electrical energy, the motor efficiency will fall into zero in the second and fourth quadrants of the torque-velocity diagram (the energy flows from the load to the motor) [26].

(2) Minor issue: high control difficulty in human-robot interaction: when the motor performs human-robot interaction tasks, its motion law is very complicated due to large fluctuations in motion frequency and amplitude, resulting in poor performance for conventional control methods such as PID, etc. Although these problems may be eliminated by proper controller compensation [27], [28], the increased control architecture complexity and additional physical sensors may increase the delay of the controller response.

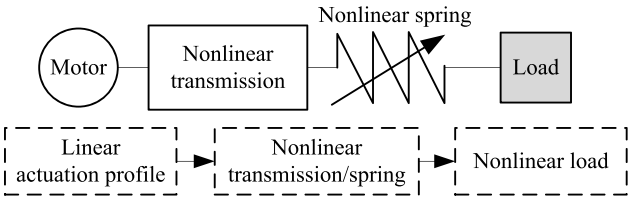

FIGURE 2. Model of the nonlinear SEA.

These inherent deficiencies of the linear SEA cannot be easily eliminated. However, by replacing its linear transmission or spring to nonlinear ones, as shown in Fig. 2, the connection relationship between the motor and the load will be changed to the nonlinear SEA, so that the above two issues might be solved naturally.

By proper mechanical design and optimization, the nonlinear SEA may enable its motor to work in a steady motion output environment while the nonlinear load is appropriately handled by the pre-designed nonlinear transmission/spring. Thus, the electric power efficiency will increase, and the control of the motor will be simplified. The nonlinear SEA can be practically realized by two ways: 1) changing the transmission mode between the load and the spring; 2) adjusting the preload or the physical properties of the spring [3], [4]. In addition, because the working condition of typical applications has characteristics of periodicity, transmissions that have periodic characteristics can be utilized to enable the unidirectional rotation of the motor, thereby simplifying the motor control.

There are some successfully implemented nonlinear SEAs capable of improving the output nonlinearity and simplifying control. For example, Inaba and Koganezawa et al. used a special-shaped cylinder to nonlinearly actuate a helical spring, which can mimic the nonlinear elasticity of the human muscle [29], [30]. Migliore et al. used the nonlinear contour

to realize the nonlinear elasticity of their SEA [31], [32], while Tonietti *et al.* [33] and Hurst *et al.* [34] used pulleys to form the nonlinear SEAs. Although these nonlinear SEAs are actuated by different transmission mechanisms, they are all able to mimic the expected underlying bionic dynamics. Moreover, Lan et al. combined a roller and a cantilever with a unique curve profile to form a new nonlinear SEA, thus generating the desired output torque corresponding to the predefined deflection-torque trajectory [35].

These aforementioned nonlinear SEAs all perform well in their corresponding applications. However, their motors still work in multidirectional motions, which may increase their electrical power consumption and require extra controller compensation for robust control. Although there are some linear SEAs with unidirectional motion characteristics [36]–[38], they just used the unidirectional motor or transmission. Their electric power efficiency may still be low in actuating nonlinear load. Therefore, this paper tries to use a cam-based nonlinear transmission that has periodic characteristics to realize a new prosthesis-integrated nonlinear SEA, thereby enabling the unidirectional motor rotation to reduce its electric power consumption and simplifying control.

The rest of this paper is organized as follows: Section II presents the modeling and optimization of the proposed nonlinear SEA; Section III is the result and discussion. Section IV shows the experimental implementation, and Section V concludes the paper.

II. MODELING AND OPTIMIZATION

Compared with the nonlinear-spring-based SEA, the nonlinear-transmission-based SEA is more suitable to realize the periodic nonlinearity of the prosthetic knee joint. The most commonly used nonlinear transmission mechanisms are the linkage mechanism, the non-circular gears, the cam mechanism, and the combined mechanism, etc. These mechanisms have the advantages of compact structure, high reliability, and low failure rate. Hence, they have been widely used in mechanical devices among various industries.

Compared with other nonlinear transmission mechanisms, the cam mechanism has fewer design constraints, and its cam profile can be freely designed according to the requirement of the nonlinear output. Some implemented elastic actuators used the cam mechanism to develop the nonlinear transmission. For example, Wolf et al. designed a compact nonlinear SEA by one floating spring and two superimposed cam mechanisms [39], and Mathijssen et al. used the cylindrical cam mechanism to realize the unlimited subsequent spring recruitment in the series-parallel elastic actuator [40]. In addition, Realmuto *et al.* [41] and Gao *et al.* [42], [43] reduced the actuating torque of the prosthetic ankle joint with the help of nonlinear cam-based parallel elastic actuation. However, most cam mechanisms in these applications are incomplete cams, and motors of these cam-based nonlinear elastic actuators still rotate multi-directionally. Therefore, in this section, a nonlinear unidirectional cam-based SEA is proposed for the actuation of the prosthetic knee joint in level-ground walking.

A. MODELING OF THE NONLINEAR CONJUGATE-CYLINDRICAL-CAM-BASED SEA (N3CSEA)

The plate cam and the cylindrical cam are commonly used in cam mechanisms. Because the cylindrical cam is slim and can be integrated into the cavity of the prosthetic knee joint, this paper will use the cylindrical cam to realize the N3CSEA. The schematic diagram of the proposed model is depicted in Fig. 3.

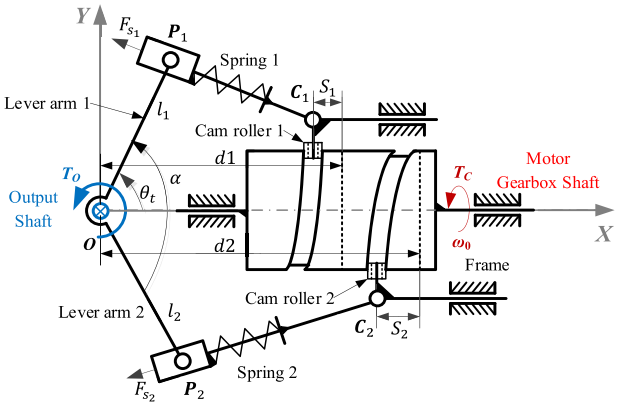

FIGURE 3. Model of the nonlinear conjugate-cam-based SEA.

In Fig. 3, the N3CSEA consists of the cylindrical cam 1 and 2, the spring 1 and 2, the lever arm 1 and 2, the motor and the output shaft O. The cylindrical cam 1 and 2 are one conjugate cam. The lever arms 1 and 2 are dual sides of one rigid linkage that rotate around the output shaft O. The motor drives the conjugate cylindrical cam 1 and 2 simultaneously at a constant speed ω_0, thereby pushing the cam roller C_1 and C_2 to reciprocate along their frame grooves. The spring 1 and 2 are respectively hinged with the cam roller 1 and 2, which will deform to drive the lever arm 1 and 2. By designing proper cam profiles for two conjugate cylindrical cams, the N3CSEA will output required actuation torque for the prosthetic knee joint.

The N3CSEA design has three essential advantages:

(1) The cam mechanism can transform the nonlinear motion of the load to a uniform one after the proper design of the cam profile, thereby enabling the motor to work in a uniform motion profile near its rated speed. Thus, the electrical power efficiency can be improved while the electrical power consumption of the N3CSEA can be reduced.

(2) A complete cam mechanism has the characteristics of periodicity, so the motor of the N3CSEA can rotate unidirectionally to realize the periodic motion of the prosthetic knee joint. Thus, the energy loss caused by inertial torques can be reduced and the motor control can be simplified.

(3) The driving torques of the stance phase and the swing phase differ in magnitude [stance:-16∼48N · m@70kg,

swing:-15∼15N · m@70kg], which will cause the difficulty of phase switching for a single actuator [44]. However, the N3CSEA can utilize the phase-following characteristics of conjugate cams to realize the alternate actuation of the stance phase and the swing phase, thus achieving seamless switching of walking phases in level-ground walking.

To realize alternate actuation of the prosthetic knee joint in the stance and the swing phase, two conjugate cams, and their helical springs need to be driven actively or passively in their assigned phases. In this paper, the cam 1 and the spring 1 are set responsible for the actuation in the stance phase, while the cam 2 and the spring 2 are responsible for the actuation in the swing phase. The timing diagram of this alternate operation can be observed in Fig. 4.

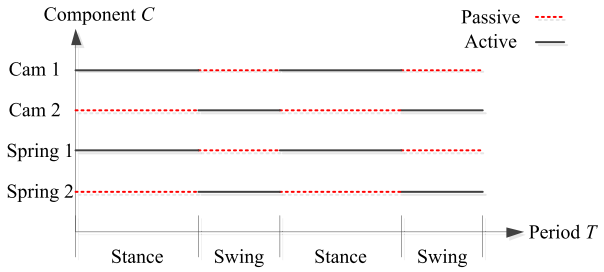

FIGURE 4. The timing diagram of operations for each conjugate cam and spring.

As shown in Fig. 4, after entering the stance phase, the conjugate cam 1 actively drives the deformed spring 1 to provide the actuating torque for the prosthetic knee, while the conjugate cam 2 passively follow the conjugate cam 1 with the spring 2 undeformed. In the swing phase, the conjugate cam 2 actively drives the deformed spring 2 to provide the actuating torque, while the conjugate cam 1 passively follow the conjugate cam 2 with the spring 1 undeformed. By using this alternate actuation, the prosthetic knee joint will be able to achieve seamless switching of stance and swing in level-ground walking.

B. KINEMATICS AND DYNAMICS ANALYSIS OF THE N3CSEA

1) SOLVING CAM PROFILES OF CONJUGATE CYLINDRICAL CAMS

As shown in Fig. 3, the output shaft is set as the origin of the coordinates, and the horizontal frame is set as the X axis. Let the initial angle of the lever arm 1 be θ_{t0}, then the angle of the lever arm 1 at any moment will be

$$\theta_t = \theta_{t0} + \theta_O \tag{1}$$

where θ_O is the current angle of the output shaft.

The position of the endpoint P_1 of the lever arm 1 will be

$$x_{P_1} = l_1 cos\,\theta_t, \quad y_{P_1} = l_1 sin\,\theta_t \tag{2}$$

where l_1 and θ_t represent the length and the angle of the lever arm 1.

The position of the cam roller 1 is

$$x_{C_1} = d_1 - S_1, \quad y_{C_1} = r_1 \tag{3}$$

where d_1 is the axial distance between the design reference of the cylindrical cam 1 and the output shaft O; S_1 is the current displacement of the cylindrical cam 1; r_1 represents the cylindrical radius of the cylindrical cam 1.

The endpoint P_2 of the lever arm 2 is

$$x_{P_2} = l_2 cos(\theta_t - \alpha), \quad y_{P_2} = l_2 sin(\theta_t - \alpha) \tag{4}$$

where l_2 is the length of the lever arm 2, and α is the fixed angle between the lever arm 1 and 2.

The position of the cam roller 2 is

$$x_{C_2} = d_2 - S_2, \quad y_{C_2} = -r_2 \tag{5}$$

where d_2 is the axial distance between the design reference of the cylindrical cam 2 and the output shaft O; S_2 is the displacement of the cylindrical cam 2; r_2 represents the cylindrical radius of the cylindrical cam 2.

Then the current lengths of the helical springs 1 and 2 will be

$$\begin{cases} l_{s_1} = \sqrt{(x_{P_1} - x_{C_1})^2 + (y_{P_1} - y_{C_1})^2} \\ l_{s_2} = \sqrt{(x_{P_2} - x_{C_2})^2 + (y_{P_2} - y_{C_2})^2} \end{cases} \tag{6}$$

The force of the spring 1 on the lever arm 1 and the force of the spring 2 on the lever arm 2 will be

$$\begin{cases} F_{S_1} = k_1 \left(l_{s_{10}} - l_{s_1}\right) - c_1 \dfrac{dl_{s_1}}{dt} \\ F_{S_2} = k_2 (l_{s_{20}} - l_{s_2}) - c_2 \dfrac{dl_{s_2}}{dt} \end{cases} \tag{7}$$

where $[l_{s_{10}}, l_{s_{20}}]$, $[k_1, k_2]$ and $[c_1, c_2]$ are the original lengths, the stiffness, and the damping coefficients of the spring 1 and 2, respectively.

Then the torques on the output shaft O of the lever arm 1 and 2 will be

$$\begin{cases} T_1 = F_{S_1} l_1\, sin\, \left(\theta_{F_{S1}} - \theta_t\right) \\ T_2 = F_{S_2} l_2\, sin\, (\theta_{F_{S2}} - (\theta_t - \alpha)) \end{cases} \tag{8}$$

where $\theta_{F_{S1}}$ represents the direction of the force F_{S_1}, and $\theta_{F_{S2}}$ represents the direction of the force F_{S_2}.

The total torque obtained on the output shaft O is

$$\begin{cases} T_O = T_1 - I\ddot{\theta}_O; T_2 = 0, (stance\ phase) \\ T_O = T_2 - I\ddot{\theta}_O; T_1 = 0, (swing\ phase) \end{cases} \tag{9}$$

where I represents the total moment of inertia of the lever arms 1 and 2 on the output shaft O, and $\ddot{\theta}_O$ is the angular acceleration of the output shaft O.

In summary, there are 13 parameters to be designed in the N3CSEA, namely, the lengths $[l_1, l_2]$ of lever arms 1 and 2, the distances $[d_1, d_2]$ from design references of cylindrical cams 1 and 2 to the output shaft O, the radii $[r_1, r_2]$ of cylindrical cams 1 and 2, the angle α between lever arms 1 and 2, the initial angle θ_{t0} of the lever arm 1, the stiffness $[k_1, k_2]$ of springs 1 and 2, and original lengths

$[l_{s10}, l_{s20}]$ of springs 1 and 2, and the rotation speed of the cylindrical cam ω_0. All these parameters can be expressed by equation (10).

$$X_u = [l_1, l_2, d_1, d_2, r_1, r_2, \alpha, \theta_{t0}, k_1, k_2, l_{s10}, l_{s20}, \omega_0] \quad (10)$$

After these parameters are given, the frame structure of the N3CSEA is determined. In the case where the sampling frequency of the walking cycle is n, let the discrete cam profile of the conjugate cam 1 be $S_{Ii}(i = 1, 2, \ldots, n)$, and the discrete cam profile of the conjugate cam 2 be S_{IIi} $(i = 1, 2, \ldots, n)$. Then at the i^{th} sampling point, S_{Ii} and S_{IIi} can be inversely solved by substituting the required output torque T_O and angle θ_O (which can be personalized according to different actuation profiles) into equations (1)-(10). The detailed values of the required output torque T_O and angle θ_O in one walking cycle are shown in Fig. 5, which is the needed actuation of a previously designed geared five-bar (GFB) prosthetic knee joint for a 70kg human walking at 1.3m/s [45]. Note that the actuating torque in Fig.5(a) is much larger than common knee torque profiles [46]. The reason is that it is not the knee actuating torque, but the actuating torque of one hinge in the geared five-bar mechanism.

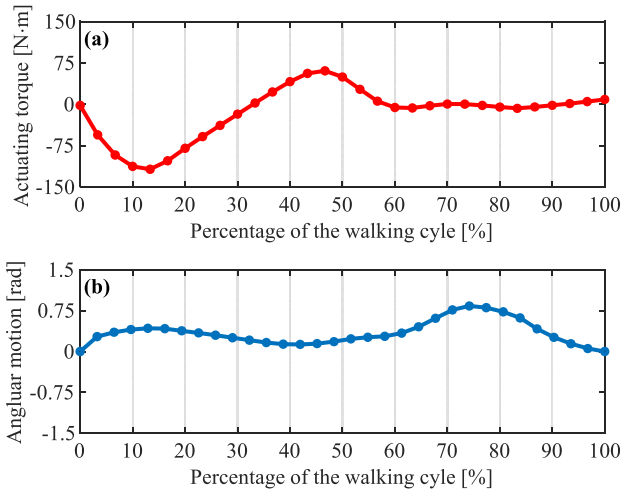

FIGURE 5. Required output (a) torque and (b) angle trajectories of the N3CSEA.

2) SOLVING THE ACTUATING TORQUE OF THE N3CSEA

Assuming that, the mass of the linkage P_1C_1 is m_{a1}, and its reaction force on the cam roller 1 is F_{cr1}; the contact force of the cylindrical cam 1 on the cam roller 1 is F_{C1}; the mass of the cam roller 1 is m_{b1}, and μ is the friction coefficient of the frame groove.

Then the force equilibrium of the cam roller 1 will be

$$\begin{cases} F_{cr1} - F_{S_1} - m_{a1}\dfrac{d^2 l_{s_1}}{dt^2} = 0 \\ F_{cr1}\cos(\theta_{F_{S1}} - \pi) - F_{C1} - m_{b1}\dfrac{d^2 s_1}{dt^2} \\ -\mu F_{cr1}\sin(\theta_{F_{S1}} - \pi) = 0 \end{cases} \quad (11)$$

By using the same analyzing method, the force equilibrium of the cam roller 2 is

$$\begin{cases} F_{cr2} - F_{S_2} - m_{a2}\dfrac{d^2 l_{s_2}}{dt^2} = 0 \\ F_{cr2}\cos(\theta_{F_{S2}} - \pi) - F_{C2} - m_{b2}\dfrac{d^2 s_2}{dt^2} \\ -\mu F_{cr2}\sin(\theta_{F_{S2}} - \pi) = 0 \end{cases} \quad (12)$$

Then the actuating torques required to actuate the cylindrical cam 1 and 2 are

$$T_{C1} = \eta F_{c1}\sin(\theta_{c1})r_1, \quad T_{C2} = \eta F_{c2}\sin(\theta_{c2})r_2 \quad (13)$$

where η represents the efficiency of the cylindrical cam.

C. OPTIMIZATION OF THE N3CSEA

The main component in the N3CSEA is the cam mechanism. Traditional design methods of the cam mechanism are based on experience, that is, according to the common laws of the cam roller, by considering the allowable pressure angle, the radius of the base circle, the radius of the curvature and other engineering factors of the cam mechanism, the cam profile is manually designed. However, it is quite possible that the actuating characteristics of the manually designed N3CSEA will perform worse than the direct actuated prosthetic knee joint. Therefore, this paper will turn these design experiences into optimization constraints and uses the optimization method to improve the actuating characteristics of the N3CSEA.

1) ANALYSIS OF OPTIMIZATION OBJECTIVES

To ensure that the value and the fluctuation of the N3CSEA motor power are as small as possible and that the actuating precision of the N3CSEA meets requirements, this paper uses the multi-objective optimization method to realize the dimension optimization of the N3CSEA.

Objective 1: The stiffness of the helical spring should not be too large. This objective is to increase the stability of the N3CSEA [47], [48]. In addition, when the stiffness of the spring is too large, a small displacement of the cam profile will cause a significant change in the output torque of the N3CSEA, which means that the controllable precision of the N3CSEA will be easily affected by assembly errors. For this optimization objective, it can be simply described as

$$\min k_i (i = 1, 2) \quad (14)$$

Objective 2: The cam profiles of two conjugate cams should be as smooth as possible so that the N3CSEA can work stably and reliably, thereby minimizing the pressure angle between mating surfaces. For this optimization objective, the smoothness of cam profiles can be assessed by the standard deviation (SD) of their radius of curvature $\rho = (1 + \dot{y}^2)^{3/2}/\ddot{y}$, where $\dot{y}$ and $\ddot{y}$ denote $\mathrm{d}y/\mathrm{d}x$ and $\mathrm{d}^2y/\mathrm{d}x^2$,

TABLE 1. Constraints of design parameters.

No.	Constraint	Description
1	$0.01\text{m} \leq [l_1, l_2] \leq 0.05\text{m}$	N3CSEA size limit
2	$0.05\text{m} \leq [d_1, d_2] \leq 0.3\text{m}$	N3CSEA size limit
3	$0.02\text{m} \leq [r_1, r_2] \leq 0.04\text{m}$	Cylindrical cam size limit
4	$90^\circ \leq \alpha \leq 180^\circ$	Position limits of two lever arms
5	$45^\circ \leq \theta_{t0} \leq 90^\circ$	Position limit of lever arm 1
6	$0.01\text{m} \leq [l_{s1}, l_{s2}] \leq 0.3\text{m}$	Helical spring size limit
7	$1\text{kN/m} \leq [k_1, k_1] \leq 100\text{kN/m}$	Helical spring stiffness limit

respectively. i.e.

$$\begin{cases} \min \sqrt{\frac{\sum_1^n (\rho_{S_{Ii}} - \overline{\rho_{S_I}})^2}{n-1}} \\ \min \sqrt{\frac{\sum_1^n (\rho_{S_{IIi}} - \overline{\rho_{S_{II}}})^2}{n-1}} \end{cases} \tag{15}$$

Objective 3: The total consumed power of the N3CSEA should be as small as possible, thereby enhancing its energy efficiency. In addition to the output mechanical power, the total consumed power of the N3CSEA also includes the wasted power due to the winding joule heating and the viscous friction in the motor [49]. This optimization objective can be expressed as equations (16) and (17), where $P_{C1i} = T_{C1i}\omega_i + (T_{C1i}/G/K_m)^2 R + B(G\omega_i)^2 (stance)$ and $P_{C2i} = T_{C2i}\omega_i + (T_{C2i}/G/K_m)^2 R + B(G\omega_i)^2 (swing)$; ω_i represents the discrete angular velocity of the conjugate cylindrical cam, which equals ω_0; $[K_m, R, B, G]$ are the torque constant, the terminal resistance, the viscous friction coefficient, and the gearbox transmission ratio of the motor in N3CSEA.

$$\begin{cases} \min \sum_1^n (P_{C1i})^2 \\ \min \sum_1^n (P_{C2i})^2 \end{cases} \tag{16}$$

$$\begin{cases} \min \sqrt{\frac{\sum_1^n (\rho_{P_{C1i}} - \overline{\rho_{P_{C1}}})^2}{n-1}} \\ \min \sqrt{\frac{\sum_1^n (\rho_{P_{C2i}} - \overline{\rho_{P_{C2}}})^2}{n-1}} \end{cases} \tag{17}$$

2) ESTABLISHMENT OF OPTIMIZATION CONSTRAINTS

The optimization constraints include constraints of the design parameter and the operation parameter. The design parameters refer to the parameters in equation (10), while the operation parameters refer to vital intermediate variables within the optimization process, such as the radius of curvature of the cam profile, and the position interference between two conjugate cams. Only by meeting both the constraints of the design parameters and the operating parameters at the same time, the optimized N3CSEA shall have practical significance.

a) Constraints of design parameters: as shown in Table 1.

b) Constraints of operation parameters:

- The radius of curvature of the cam profile is greater than the cam roller;
- There is no interference between two cylindrical cam profiles.

The radius of curvature of the cam profile can be described by equation (18)

$$\rho = \frac{[(\frac{dx}{d\delta})^2 + (\frac{dy}{d\delta})^2]^{\frac{3}{2}}}{\frac{dx}{d\delta} \cdot \frac{d^2y}{d\delta^2} - \frac{dy}{d\delta} \cdot \frac{d^2x}{d\delta^2}} \tag{18}$$

where δ is the rotation angle of the cam, and $[x, y]$ are the theoretical coordinates of the cam profile at the rotation angle δ. The inverse of equation (18) is the curvature of the cam.

Therefore, to ensure the radius of curvature of the theoretical cylindrical cam profile is higher than the cam roller, the constraints are given as

$$\rho_{1i} > r_{cc}, \quad \rho_{2i} > r_{cc} \tag{19}$$

where ρ_{1i} and ρ_{2i} represent the ith discrete radii of curvature of the cam profile 1 and 2; r_{cc} represents the radius of the cam roller. In this paper, the minimum r_{cc} is given as 0.005m.

To ensure that there is no interference between two cylinder cams, the maximum displacement of one cylindrical cam profile must be less than the minimum displacement of another cylindrical cam profile, or vice versa, i.e.

$$\begin{aligned} &\min (S_{Ii} + d_1) > \max (S_{IIi} + d_2) \\ &\text{or } \max (S_{Ii} + d_1) < \min (S_{IIi} + d_2) \end{aligned} \tag{20}$$

However, if two cylindrical cams exit on the outer and inner walls of the cylinder respectively, there will be no need to add this constraint.

3) ESTABLISHMENT OF FINAL BI-OBJECTIVE OPTIMIZATION

To combine all optimization objectives together, this paper integrates optimization objectives of one cylindrical cam system into a single optimization objective by the weighted method and then finds the Pareto optimality of the bi-objective optimization for the conjugate cylindrical cam systems in the N3CSEA.

To ensure that each optimization objective of one cam system has the same effect on the final optimization result, the coefficients of each optimization objective of one single cam system are selected via multiple tests with constraints of keeping each target value on the same order of magnitude: $\zeta_1 = 2, \zeta_2 = 1, \zeta_3 = 2$ and $\zeta_4 = 2$. Therefore, the final optimization objective of the N3CSEA is given as

$$\min_{i=1,2} \begin{cases} fval_1 = \zeta_1 \sqrt{\frac{\sum_1^n (\rho_{S_{Ii}} - \overline{\rho_{S_I}})^2}{n-1}} + \zeta_2 k_1 \\ \quad + \zeta_3 \sum_1^n P_{C1i}^2 + \zeta_4 \sqrt{\frac{\sum_1^n (\rho_{P_{C1i}} - \overline{\rho_{P_{C1}}})^2}{n-1}} \\ fval_2 = \zeta_1 \sqrt{\frac{\sum_1^n (\rho_{S_{IIi}} - \overline{\rho_{S_{II}}})^2}{n-1}} + \zeta_2 k_2 \\ \quad + \zeta_3 \sum_1^n P_{C2i}^2 + \zeta_4 \sqrt{\frac{\sum_1^n (\rho_{P_{C2i}} - \overline{\rho_{P_{C2}}})^2}{n-1}} \end{cases}$$
$$\text{Subject to : Table 1 \& Eq.}(19-20) \tag{21}$$

III. RESULTS AND DISCUSSION

A. OPTIMIZATION RESULT OF N3CSEA

By using the improved genetic annealing algorithm (IGAA) combined with the region search (RS) method [50], the parameters of the N3CSEA are obtained. The optimization parameters of IGAA is listed in Table 2, and the motor information used in the optimization is listed in Table 3.

TABLE 2. Optimization parameters of IGAA.

Population size	50~200
Iterative steps	500~1000
Selection probability	$p = k\left((f_{max} - f)/(f_{max} - f_{min})\right)^i$
i^{th} generation mutation rate	$p_i = (1 + k_i)/\sum_{1\sim5}^{j}(1 + k_j)$
Initial temperature	$t_0 = (f_{min} - f_{max})/\ln p_r$
Search step size	$x_{new} = x_{old} + hW$

f_{max}, f_{min}: maximum and minimum target value in the initial population;
p_r: initial worst acceptance probability;
h: search step
W: disturbance caused by Logistic mapping.

TABLE 3. Motor specifications.

Motor	Maxon Re 40
Torque constant	6.03e-2N·m/A
Terminal resistance	1.13Ω
Viscous friction coefficient	5.20e-06 N·m/(rad/s)
Transmission ratio	156:1
Rotor/transmission inertia	1.37e-05kgm^2/9.10e-07kgm^2

TABLE 4. Optimal parameters of the N3CSEA (length unit: mm; stiffness unit: N/m; angle unit: rad; angular speed unit: rad/s).

l_1	l_2	r_1	r_2	d_1	d_2	ω_0
0.050	0.023	0.040	0.020	0.088	0.099	5.027
$l_{s_{10}}$	$l_{s_{20}}$	k_1	k_2	α	θ_{t0}	
0.089	0.155	9.750e4	8.582e3	3.142	1.571	

The optimal parameters of the N3CSEA are shown in Table 4.

In Table 4 all dimension parameters of the N3CSEA are within an acceptable range. The radius of the first cylindrical cam is bigger than that of the second cylindrical cam, which means that two cylindrical cams can be realized on the inner and outer walls of one cylinder respectively. In addition, the stiffness of the spring for the stance phase has a larger magnitude than that of the spring for the swing phase. Therefore, each spring in the N3CSEA is able to deform in a suitable degree to generate desired actuating torques with satisfying mechanical accuracy for each walking phase.

The graphical cam profiles of two conjugate cylindrical cams are shown in Fig. 6.

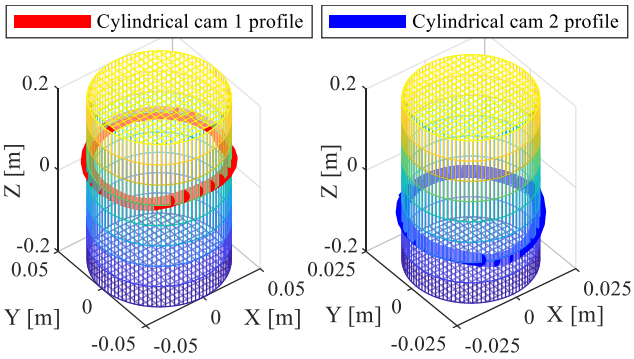

FIGURE 6. Graphical cam profiles of conjugate cylindrical (a) cam 1 and (b) cam 2.

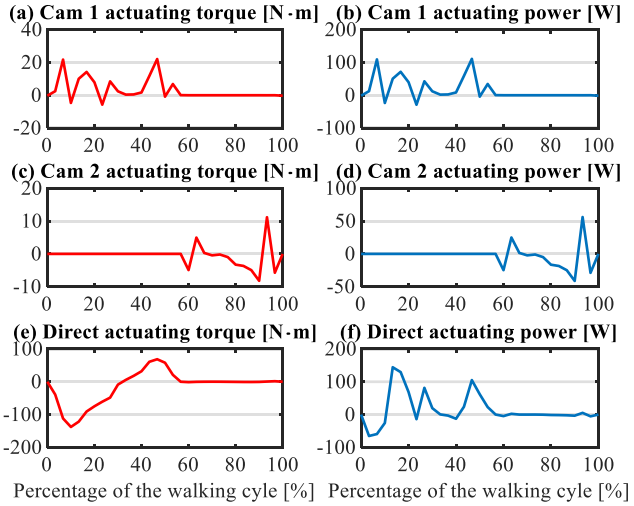

FIGURE 7. Characteristics of (a) the actuating torque of the conjugate cam 1, (b) the actuating power of the conjugate cam 1, (c) the actuating torque of the conjugate cam 2, (d) the actuating power of the conjugate cam 2, (e) the direct actuating torque of the prosthetic knee joint, and (f) the direct actuating power of the prosthetic knee joint.

B. ACTUATING CHARACTERISTICS OF N3CSEA

The actuating torques and actuating powers of each conjugate cam in the N3CSEA are shown in Fig. 7.

It is known from Fig. 7 that, when the prosthetic knee joint is directly actuated by the motor, the peak actuating torque and the peak actuating power have reached almost 100N·m and 150W, respectively. However, when the prosthetic knee joint is driven by the N3CSEA, the peak actuating torque and peak actuating power of the cam 1 (responsible for the stance phase) are reduced to approximately 20N·m and 100W, respectively. The peak actuating torque and peak actuating power of the cam 2 (responsible for the swing phase) are reduced to approximately 10N·m and 50W, respectively. These results indicate that the energy consumption of the prosthetic knee joint is effectively reduced by using the N3CSEA for the prosthetic actuation.

In addition, the motor speed of the N3CSEA is only linearly related to the walking speed of the prosthetic knee joint, i.e., when the N3CSEA actuated prosthetic knee joint walks

at the designed speed or other fixed speeds, the motor will work in the state of uniform rotation near its nominal speed, which can effectively reduce the complexity of motor control. Under normal circumstances, amputees tend to walk at their habitual speed, which means that the motor of the N3CSEA will operate near its nominal condition.

C. ACTUATION COMPARISON OF N3CSEA AND LINEAR SEA

To demonstrate the superiority of the N3CSEA over conventional linear SEA, this paper built a theoretical model of the linear SEA, namely LSEA (the model is based on Fig. 1), and optimized its parameters for the same actuation profile in Fig. 5. The transmission efficiencies of both the N3CSEA and the LSEA are not considered to ensure the theoretical fairness of comparison. The optimization information is the same as that of the N3CSEA, and the optimized result of the LSEA is $k = 8.74\text{e}3$ N·m/rad.

The specific comparison results of the N3CSEA and the LSEA are depicted in Fig. 8.

It can be obtained from Fig. 8 (a) and Fig. 8(b) that the actuating torque of the N3CSEA is much smaller than that of the LSEA, and the linear SEA has minimal effect on the reduction of the original actuating torque [Fig. 8(b) vs. Fig. 7(e)].

The design advantage of the N3CSEA is that its motor can rotate unidirectionally at a constant speed when the N3CSEA works under its rated condition [Fig. 8(c)], while the motor of LSEA needs to track the complex motion of the load to realize the required series elastic actuation [Fig. 8(d)]. The distinction between the output mechanical powers of the N3CSEA and the LSEA [Fig. 8(e) vs. Fig.8(f)] is mainly caused by the difference between the force-speed transformation of the cam mechanism in the N3CSEA and the linear transmission in the LSEA.

It is noticed from Fig. 8(e) that there exists negative power within a walking cycle. This means that the mechanical energy can flow from the load to the motor if its controller is able to regenerate electrical energy. Because the motor of the N3CSEA rotates unidirectionally at a constant speed (near the rated speed of the motor), the energy loss caused by its motor viscous friction remains a constant, which is larger than that of the LSEA [Fig. 8(g) vs. Fig.8(h)]. However, these tiny energy losses are insignificant when compared with the total consumed power of both the N3CSEA and the LSEA systems.

In a motor actuation system, the motor rotor and the transmissions such as gears or screws will generate inertial power of $P_{\text{MOI}} = J\dot{\omega}$ (where J is the equivalent moment of inertia of the motor rotor and the transmission at the load end, and ω is the rotation speed of the load). When the motor system is driven by a motor controller that has the function of electrical energy regeneration [51], the total electrical energy consumption of P_{MOI} within a prosthetic walking cycle is zero, as the inertial energy can be retrieved by either the load or the motor controller. However, when using a motor controller without electrical energy regeneration,

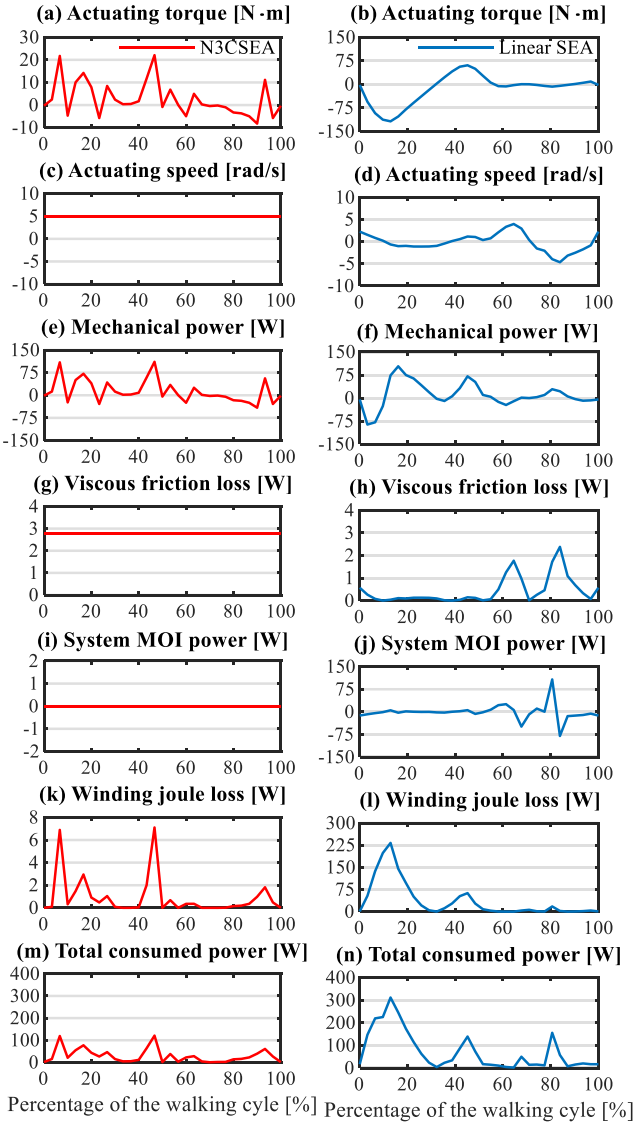

FIGURE 8. Comparison results of the N3CSEA and the linear SEA. (a) and (b): Actuation torques; (c) and (d): Actuation speeds; (e) and (f): Output mechanical power; (g) and (h): Energy losses by viscous frictions in motors; (i) and (j): Energy cost of moment of inertia (MOI) of motor rotor and transmissions; (k) and (l): Energy losses by winding joule heating in motors; (m) and (n): Total consumed power.

it cannot retrieve this inertial energy. Hence, extra energy needs to be provided for motor brake, which results in extra electrical energy loss. In addition, even if the motor is driven by controllers with electrical energy regeneration, its inertial energy may increase the instantaneous power of the system, thereby affecting the peak power of the motor system.

For the LSEA, it needs to track the nonlinear motion of the load in Fig. 5(b), which results in large extra P_{MOI} power in one prosthetic walking cycle, as shown in Fig. 8(j). However, when the N3CSEA works under its rated condition, the nonlinear motion of the load is transformed into a uniform motion via the specially designed cam mechanism. There will be no fluctuations in the rotating speeds of the motor rotor and the

linear transmissions, leading to zero P_{MOI} power, as shown in Fig. 8(i).

The current of a DC/EC motor is linearly related to its load torque, namely the torque constant. Because the required actuating torque of the N3CSEA and the LSEA depicted in Fig. 8(a) and Fig. 8(b) differs a lot, the power losses of the N3CSEA and the LSEA caused by the winding joule heating show significant differences. The maximum winding joule heating loss of the N3CSEA is less than 10W, while the maximum winding joule heating loss of the LSEA reaches over 200W. This unrealistic result indicates that the LSEA needs a more powerful motor to achieve its actuation.

Form Fig.8(e, g,i, k), it can be found that the negative power state duration of the N3CSEA is smaller than the positive one, and the amplitude of the negative power is much smaller than the positive one. These features of the N3CSEA indicate that using motor controllers without electrical energy regeneration will not cause a significant decrease in the electrical power efficiency of the system. Therefore, the total consumed powers of the N3CSEA and the LSEA are calculated without electrical energy regeneration, as shown in Fig. 8(m) and Fig. 8(n). It can be concluded that the N3CSEA consumes much less energy than the LSEA, which demonstrate the superiority of the N3CSEA. The essential reason for this N3CSEA advantage is that its cam system can achieve expected force-speed transformation as effectively as an automatic transmission, allowing the motor to operate near its rated condition.

D. MOTOR ELECTRICAL EFFICIENCY OF N3CSEA

The electrical power efficiency of the motor of the N3CSEA can be represented by the ratio of its output mechanical power to its total electrical power (motor mode) or the ratio of its generated electric power to its mechanical load (generator mode if the motor controller is able to regenerate electrical energy). The motor electrical power efficiency is mainly affected by Joule heating loss and viscous friction loss. According to Verstraten *et al.* [26], the motor (Table 3) electrical power efficiency of the N3CSEA (using the motor controller with the electrical energy storage function) is calculated and depicted in Fig. 9.

It can be noticed from Fig. 9(a) that the N3CSEA motor efficiency remains in the I and IV quadrants as a vertical line due to its pre-designed characteristics of constant motor speed, where the motor efficiency near the X-axis junction of the first and fourth quadrants are lower. To further investigate the motor efficiency around this area, the motor efficiency within a walking cycle is studied and depicted in Fig. 9(b).

It can be obtained from Fig. 9(b) that the motor efficiency within a walking cycle will decrease when the motor torque is near the X-axis. The reason behind this phenomenon is that when the required output motor torque is low, the vicious friction will cause a large percentage of energy loss and result in low motor efficiency. However, low motor efficiency does not mean the total energy consumption will certainly become higher. It can be noticed from Fig. 8(g) the vicious friction

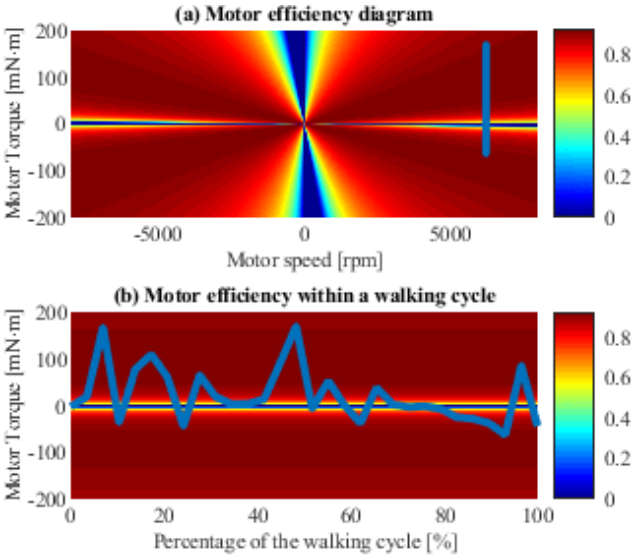

FIGURE 9. (a) Motor efficiency. (b) Motor efficiency within a walking cycle. Note that the motor controller has the function of electrical energy regeneration.

loss of the N3CSEA motor is less than 3W, which means that when the motor efficiency is low, the required output mechanical power will also remain low. This indicates that the impact of motor efficiency on N3CSEA energy consumption is less critical.

The motor efficiency depicted in Fig. 9 is under the condition of using the motor controller with electrical energy regeneration, which means the energy can either flow from the motor to the load or vice versa. When the motor controller does not have the function of electrical energy regeneration, the motor efficiency in the fourth quadrant of Fig.9(a) and the negative Y-axis area of Fig.9(b) will be zero, which means that when the load drives the motor, the motor controller needs to provide extra energy for either actuation or brake compensation. However, it can be noticed from Fig.9(b) that the proportion and the magnitude of the negative motor torque within a walking cycle is much smaller than that of the positive motor torque, which indicates the negative impact of using motor controllers without electrical energy regeneration will not contribute to large energy loss for N3CSEA actuation.

E. GAIT SENSITIVITY OF THE N3CSEA

To make the N3CSEA adapt to various walking speed, a corresponding adjustment of the motor speed is necessary. However, adjusting the speed of the motor can only ensure the N3CSEA keep up with the walking pace. The corresponding prosthetic actuating torque cannot be fully guaranteed as the cam mechanism in the N3CSEA can only provide predefined actuating characteristics, thereby affecting the actual gait of the prosthetic knee joint. The actuating torque required by the lower extremity varies under different walking speeds, so the N3CSEA that has predefined characteristics of output torques

may reduce the lower limb gait symmetry in the level-ground walking.

To investigate the N3CSEA influence on the prosthetic gait over different walking speed, this paper analyzed the required actuating torque of the lower extremity at three different speeds: normal speed 1.30m/s, fast speed 1.56m/s, and slow speed 1.04m/s. The normal speed refers to the reference walking speed of the lower extremity for the N3CSEA, while the fast and slow walking speeds represent 20% faster and slower than the normal walking speed, respectively. By performing dynamics analysis of the lower extremity via the walking model built in the MSC Adams simulation software, the required actuating torques provided by the prosthetic knee joint at different walking speeds are shown in Fig. 10(a). The root-mean-square error (RMSE) between actuating torques of fast walking and normal walking is 6.78N·m, while the RMSE between actuating torques of slow walking and normal walking is 1.83N·m.

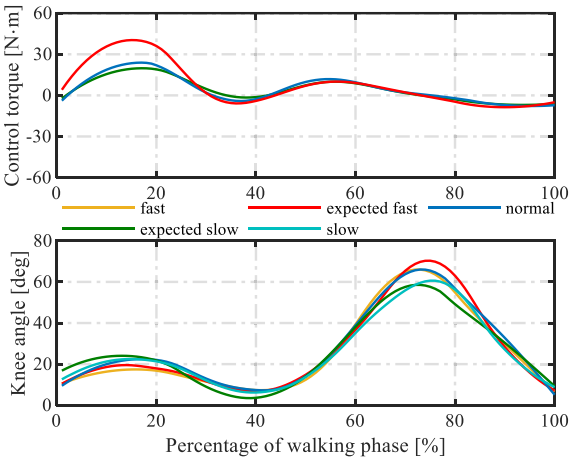

FIGURE 10. (a) Actuating torques at slow/normal/fast walking speeds. (b) Knee angles at slow/normal/fast walking speeds.

Because the predefined actuating torque provided by the N3CSEA deviates from the needs for fast/slow walking, actual lower extremity gaits will slightly differ from expected ones. The actual/expected knee angles of the lower extremity at slow/normal/fast walking speeds are obtained via kinematics simulation analysis, and the results are depicted in Fig. 10(b). The RMSEs between the expected knee angles and the actual ones at fast and slow walking speeds are 2.73deg and 2.95deg, respectively. The analysis results indicate that this magnitude of knee angle errors will not have perceptible adverse effects on walking gait symmetry.

F. KNEE JOINT STIFFNESS ANALYSIS OF N3CSEA

To further verify the practicality of the N3CSEA, it is vital to evaluate the knee stiffness of the N3CSEA [52]. A low stiffness of the prosthetic knee joint will lead to oscillations and resonance in the swing phase, and high stiffness of the prosthetic knee joint will lead to user discomfort. The knee stiffness of the N3CSEA is depicted in Fig. 11.

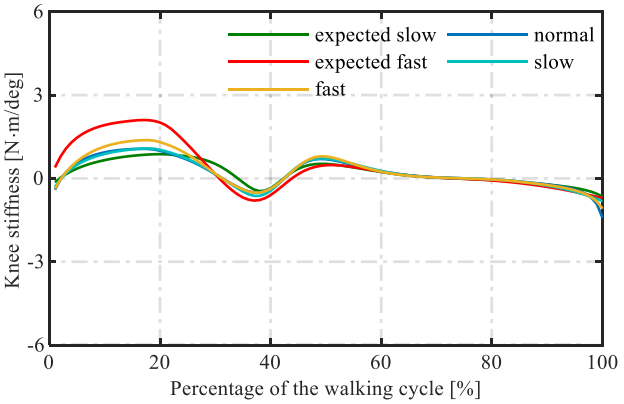

FIGURE 11. Knee stiffness at slow/normal/fast walking speeds.

As can be obtained from Fig. 11, the knee stiffness of the N3CSEA at the fast walking speed deviates a little bit larger from the expected one in the stance phase than in the swing phase, while the knee stiffness at the slow walking speeds is close to the expected one in both the stance and the swing phase. The RMSEs between the expected knee stiffness and the actual ones at fast and slow walking speeds are 0.38 N·m/deg and 0.16N·m/deg, respectively. This result indicates that the N3CSEA can provide necessary knee actuation in level-ground walking.

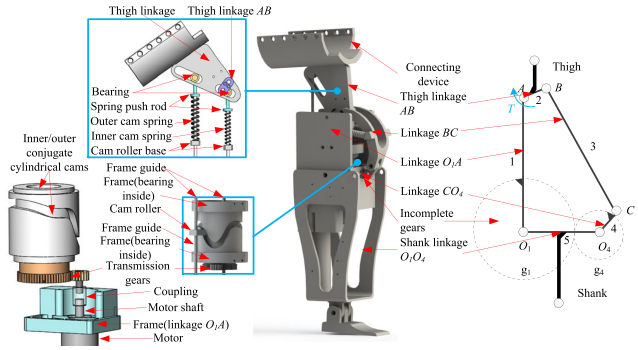

FIGURE 12. The overall structure of the N3CSEA-integrated prosthetic knee joint.

IV. EXPERIMENTAL IMPLEMENTATION

A. STRUCTURE DESIGN OF THE N3CSEA-INTEGRATED PROSTHETIC KNEE JOINT

To experimentally verify the performance of the N3CSEA, this paper builds an N3CSEA-integrated prosthetic knee joint based on a previous developed geared five-bar (GFB) prosthetic knee joint [45]. The dimension of the GFB mechanism is re-optimized by the IGAA [50] to provide better knee centrode while the motion interference between the GFB mechanism and its internal actuating space is eliminated via kinematics penalty [53]. The detailed structure of the N3CSEA-integrated prosthetic knee joint is shown in Fig. 12.

In Fig. 12, the linkage O_1A is designed as the frame with sufficient cavity for the integration of the N3CSEA. The linkage AB and the lever arms of the N3CSEA are one rigid

part, thus enabling the N3CSEA to actuate the prosthetic knee joint. The linkage BC is designed as a curved linkage to maximally avoid the interference between the linkage BC and the cam mechanism of the N3CSEA during walking. The O_4 hinge of the linkage O_4C is designed as an incomplete gear, thus forming the GFB mechanism with the incomplete gear of the linkage O_1A centered at the hinge O_1.

The cylindrical cam 1 (responsible for stance actuation) and cam 2 (responsible for swing actuation) of the N3CSEA are on the outer and inner side of the cylinder, respectively. The conjugate cylindrical cam is driven by the motor installed on the bottom side of the linkage O_1A via the gear transmission.

The upper surface of the linkage AB stays horizontal when the flexion angle of the prosthetic knee joint reaches zero, thereby enabling the installation of the connecting device (or the pyramid connector) for the prosthetic knee joint. The linkage O_1O_4 is designed as the prosthetic leg for the installation of the prosthetic ankle. Therefore, when the motor drives the N3CSEA to generate actuating torques for the linkage AB, the whole prosthetic knee joint will actuate the prosthetic leg to walk.

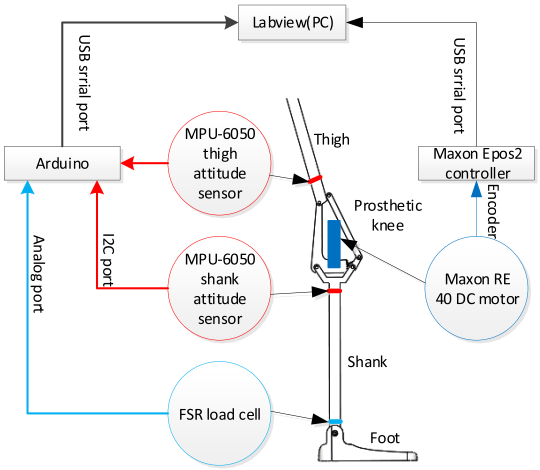

FIGURE 13. Hardware platform and software workflow of the prosthetic control.

B. CONTROL OF THE N3CSEA-INTEGRATED PROSTHETIC KNEE JOINT

1) HARDWARE AND SOFTWARE PLATFORMS

As shown in Fig. 13, the host PC that runs LabVIEW (National Instruments, USA) uses a DC motor controller (Epos2 50/5, Maxon, Switzerland) to control the brushed DC motor (RE40, Maxon, Switzerland) via a 512-line 3-channel differential incremental encoder (ML, Maxon, Switzerland) mounted at the end of the motor. A transmission gear (GP 42, Maxon, Switzerland) is mounted at the output shaft of the motor. To obtain the prosthetic knee posture, the host PC uses the Arduino to communicate with two IMU-sensors (MPU-6050, InvenSense, USA) installed on the linkage AB and O_1O_4. The walking phase of the prosthetic knee joint is determined by a load cell (Force Sensing Resistor, Interlink Electronics, USA) installed on the bottom of the linkage O_1O_4.

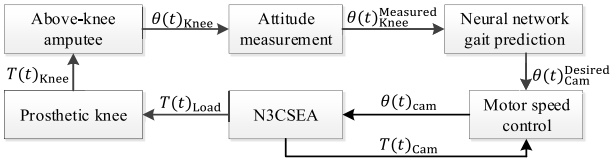

FIGURE 14. Detailed control schema of the N3CSEA-integrated prosthetic knee joint.

2) TOP-LEVEL CONTROL SCHEMA

As shown in Fig. 14, the control principle is as follows: the current angles of the prosthetic leg are obtained via the attitude measurement process, then the upcoming motion of the prosthetic knee joint is predicted by a pre-trained BP neural network ($10 \times 8 \times 5 \times 1$ structure, S-type activation function, pre-trained by 1120 training samples of seven different categories containing 75% correct data and 25% incorrect data modified with slight noise and accidental errors), which is capable of generating the predicted gait percentage for calculating the target rotation angle of the cam mechanism in the N3CSEA. The control instructions of the motor are therefore generated according to this target rotation profile, thereby actuating the N3CSEA to drive the prosthetic knee.

3) LOW-LEVEL MOTOR CONTROL

The specific motor controller architecture for the N3CSEA is shown in Fig. 15.

The controller consists of one inner current PI regulation and one outer PID position regulation. One velocity feedforward, one acceleration feedforward, and one torque feedforward are added into the controller to improve the trajectory following of the motor via additional current compensations. The torque change ΔT^{Calc}_{cam} is calculated via simple real-time inverse dynamics of the N3CSEA model with kinematics input $\theta(t)_{Load}$ from prosthetic attitude measurement. This motor controller is designed based on the fact that the motor speed fluctuation is little, but the motor torque fluctuation is huge. Therefore a proper feedforward to the current regulation is added to compensate for load changes as well as other unfavorable factors.

C. EXPERIMENTAL RESULT

The power of the prosthetic knee joint is provided by a programmable DC power supply (DP712, Rigol, China). In order for the able-bodied volunteer (height: 178cm, weight: 63kg, age: 22, the consent form was obtained prior to experiments) to wear the prosthetic knee joint, a particular connecting device is mounted on the top of the prosthetic knee joint. The able-bodied volunteer can wear the prosthetic knee joint by flexing his knee by 90°. The volunteer is asked to walk at his habitual speed (about 1.2m/s).

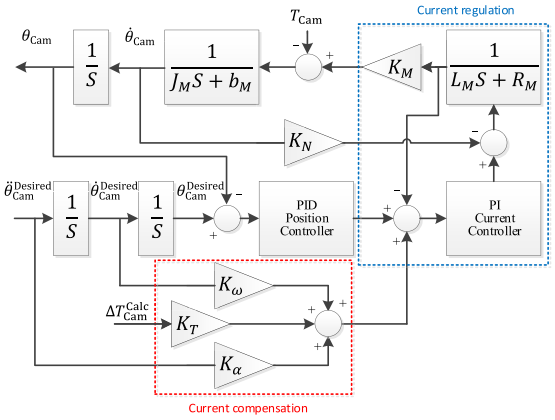

FIGURE 15. Motor controller architecture: L_m and R_m are the inductor and the resistor of the motor, and J_m and b_m are the moment of inertial and damping of the motor and transmissions; K_M and K_N are the torque constant and the speed constant of the motor, respectively; K_ω, K_τ and K_α are corresponding gains of feedforward current compensations; T_p is the needed actuating torque of the prosthetic knee, and ΔT_P^{Calc} is the calculated prosthetic torque changes by real-time inverse dynamics of the prosthetic knee.

FIGURE 16. Experimental walking gait cycle of the N3CSEA-integrated prosthetic knee joint.

Fig. 16 shows one experimental walking gait cycle of the N3CSEA-integrated prosthetic knee joint. The locomotion was captured via a highspeed USB 3.0 camera (1920*1080@150fps).

To quantitatively evaluate the experimental performance of the prosthetic knee joint, the current, the Joule losses, the speed of the motor, the electric power of the motor system, the ankle trajectory, and knee angle trajectory of the prosthetic leg are all analyzed and depicted in Fig. 17.

The motor current in Fig. 17(a) is measured via the built-in data recorder function of the Maxon Epos 2 controller, and the sampling frequency of the recorded motor current is set at 85Hz (the sampling frequency of the PI regulation is 10kHz). It can be known from Fig. 17(a) that the peak motor current during one walking gait cycle is 8.29A, which is only a little bigger than its nominal current (6A). In addition, the averaged motor current is only 1.17A, which means that the Joule heating losses of the motor during the whole walking cycle will remain in an acceptable range, as shown in Fig. 17(b).

In Fig. 17(c), the motor speed during the walking gait cycle is below its nominal speed, and there are some fluctuations in the speed curve. The reason for this phenomenon is that the walking speed of the volunteer is a little bit slower than the reference speed of the N3CSEA-integrated prosthetic knee joint. Hence, the neural network control algorithm will generate both the lower speed and the reference speed instructions to regulate the prosthetic knee speed, which introduces the fluctuation of the motor speed.

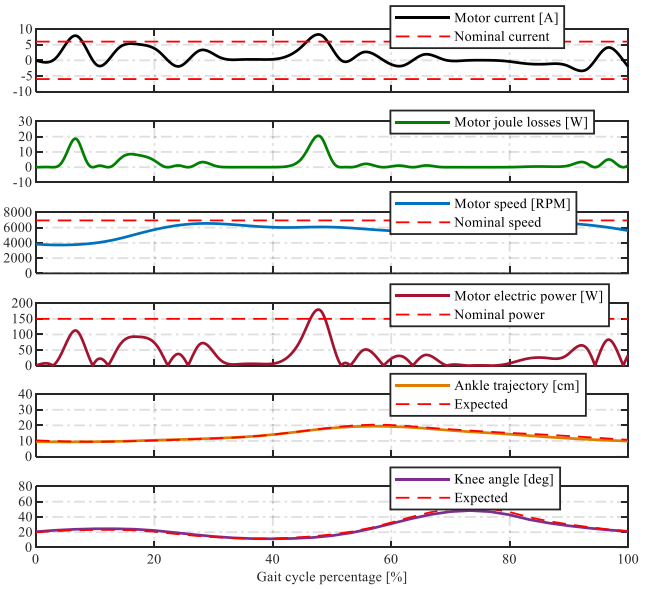

FIGURE 17. Experimental results in one walking gait cycle: (a) motor current, (b) motor joule losses, (c) motor speed, (d) electric power, (e) ankle trajectory, (f) knee angle.

In Fig. 17(d), the electric power of the motor system is obtained via the programmable DC supply through RS232 connection to LabVIEW, which means that the electric power of the motor controller is also added into consideration (the maximum efficiency of Maxon Epos 2 controller is 94%). The peak electric power that took place in the middle of the walking gait cycle is 179.77W, where the motor Joule losses also reached its maximum value 20.59W. At other times during the walking gait cycle, the electric power of the motor system is below its nominal power (150W).

Fig. 17(e) shows the measured ankle motion trajectory of the prosthetic lower extremity. The RMSE between the prosthetic ankle motion and the expected one (the ankle motion of the able-bodied volunteer himself at normal walking speed) is 2.51cm. In Fig. 17(f), the characteristics of the experimental knee angle trajectory is also similar to that of the normal walking, and the RMSE between the experimental knee angle and the expected one (the knee angle of the able-bodied volunteer himself at normal walking speed) is 2.82deg. The reasons for the slight deviation between the experimental walking gait and the expected walking gait are that: 1) the predefined output characteristics of the N3CSEA results in a little gait deviation; 2) a tighter connecting method between the prosthesis and the able-bodied volunteer is needed; 3) the passive prosthetic ankle also has an adverse effect on the gait of the lower limb prosthesis.

V. CONCLUSION

This paper proposed a new nonlinear series elastic actuator (N3CSEA) for the prosthetic knee joint based on the conjugate cylindrical cams. The parameters of the N3CSEA are optimized by the multi-objective optimization method to improve its operating characteristics. Meanwhile, the

actuating performance of the N3CSEA is theoretically analyzed and experimentally verified. Compared with conventional linear SEAs, the N3CSEA has advantages of high electric power efficiency, low electrical energy consumption, simple motor control, as well as seamless switching of walking phases in level-ground walking.

The design philosophy behind the N3CSEA is utilizing fast mechanical response and accurate mechanical nonlinearity of the cam mechanism to actuate expected nonlinear loads, thus improving the actuating characteristics of the actuator. The mechanical system has the advantage of high system stability, which will not easily fall into malfunctions when compared with algorithm-based systems. However, every coin has two sides. The mechanical system also has the limitation that it cannot be easily adjusted. The proposed N3CSEA, has predefined nonlinear output torque, which limits support for multiple walking conditions such as stairs, ramps, etc., in its current form. Future works of this paper will focus on realizing the adjustable nonlinearity of the N3CSEA via adjustable cam profiles, thus improving its practicality in daily walking.

REFERENCES

[1] G. A. Pratt and M. M. Williamson, "Series elastic actuators," in *Proc. IEEE/RSJ Int. Conf. Intell. Robots Syst. Hum. Robot Interact. Cooperat. Robots*, vol. 1, Aug. 1995, pp. 399–406.

[2] G. A. Pratt, M. M. Williamson, P. Dillworth, J. E. Pratt, and A. Wright, "Stiffness isn't everything," in *Proc. Int. Symp. Experim. Robot.*, 1995, pp. 253–262.

[3] R. Ham, T. G. Sugar, B. Vanderborght, K. W. Hollander, and D. Lefeber, "Compliant actuator designs," *IEEE Robot. Autom. Mag.*, vol. 16, no. 3, pp. 81–94, Sep. 2009.

[4] B. Vanderborght *et al.,* "Variable impedance actuators: A review," *Robot. Auto. Syst.*, vol. 61, no. 12, pp. 1601–1614, Dec. 2013.

[5] S. Wolf, G. Grioli, O. Eiberger, W. Friedl, M. Grebenstein, H. Höppner, E. Burdet, D. G. Caldwell, R. Carloni, M. G. Catalano, D. Lefeber, S. Stramigioli, N. Tsagarakis, M. Van Damme, R. Van Ham, B. Vanderborght, L. C. Visser, A. Bicchi, and A. Albu-Schäffer, "Variable stiffness actuators: Review on design and components," *IEEE/ASME Trans. Mechatronics*, vol. 21, no. 5, pp. 2418–2430, Oct. 2016.

[6] M. Grimmer, M. Eslamy, and A. Seyfarth, "Energetic and peak power advantages of series elastic actuators in an actuated prosthetic leg for walking and running," *Actuators*, vol. 3, no. 1, pp. 1–19, 2014.

[7] M. Grimmer and A. Seyfarth, "Stiffness adjustment of a series elastic actuator in an ankle-foot prosthesis for walking and running: The trade-off between energy and peak power optimization," in *Proc. IEEE Int. Conf. Robot. Autom.*, May 2011, pp. 1439–1444.

[8] S. K. Au, J. Weber, and H. Herr, "Biomechanical design of a powered ankle-foot prosthesis," in *Proc. IEEE Int. Conf. Rehabil. Robot.*, Jun. 2007, vol. 15, no. 3, pp. 298–303.

[9] S. K. Au, J. Weber, and H. Herr, "Powered ankle–foot prosthesis improves walking metabolic economy," *IEEE Trans. Robot.*, vol. 25, no. 1, pp. 51–66, Feb. 2009.

[10] C. Lagoda, A. C. Schouten, A. H. A. Stienen, E. E. G. Hekman, and H. V. D. Kooij, "Design of an electric series elastic actuated joint for robotic gait rehabilitation training," in *Proc. IEEE Ras Embs Int. Conf. Biomed. Robot. Biomechtron.*, Sep. 2010, pp. 21–26.

[11] N. Paine and L. Sentis, "A new prismatic series elastic actuator with compact size and high performance," in *Proc. IEEE Int. Conf. Robot. Biomimetics*, Dec. 2012, pp. 1759–1766.

[12] N. Paine, S. Oh, and L. Sentis, "Design and control considerations for high-performance series elastic actuators," *IEEE/ASME Trans. Mechatronics*, vol. 19, no. 3, pp. 1080–1091, Jun. 2014.

[13] J. F. Veneman, R. Ekkelenkamp, R. Kruidhof, F. C. T. Van Der Helm, and F. C. T. Van Der Helm, "A series elastic- and Bowden-cable-based actuation system for use as torque actuator in exoskeleton-type robots," *Int. J. Robot. Res.*, vol. 25, no. 3, pp. 261–281, Mar. 2006.

[14] T. Zhang and H. H. Huang, "A lower-back robotic exoskeleton: Industrial handling augmentation used to provide spinal support," *IEEE Robot. Automat. Mag.*, vol. 25, no. 2, pp. 95–106, Jun. 2018.

[15] T. Zhang, M. Tran, and H. Huang, "Design and experimental verification of hip exoskeleton with balance capacities for walking assistance," *IEEE/ASME Transactions on Mechatronics*, vol. 23, no. 1, pp. 274–285, Feb. 2018.

[16] D. Accoto, G. Carpino, F. Sergi, N. L. Tagliamonte, L. Zollo, and E. Guglielmelli, "Design and Characterization of a Novel High-Power Series Elastic Actuator for a Lower Limb Robotic Orthosis," *Int. J. Adv. Robot. Syst.*, vol. 10, no. 359, pp. 1–12, Jan. 2013.

[17] G. Carpino, D. Accoto, F. Sergi, N. L. Tagliamonte, and E. Guglielmelli, "A novel compact torsional spring for series elastic actuators for assistive wearable robots," *J. Mech. Des.*, vol. 134, no. 12, Dec. 2012, Art. no. 121002.

[18] Y. Kim, J. Lee, and J. Park, "Compliant joint actuator with dual spiral springs," *IEEE/ASME Trans. Mechtron.*, vol. 18, no. 6, pp. 1839–1844, Dec. 2013.

[19] S. Ates, V. I. Sluiter, P. Lammertse, and A. H. A. Stienen, "Servo SEA concept: Cheap, miniature series-elastic actuators for orthotic, prosthetic and robotic hands," in *Proc. 5th IEEE RAS/EMBS Int. Conf. Biomed. Robot. Biomechtron.*, Aug. 2014, pp. 752–757.

[20] H. Zheng and X. Shen, "Design and control of a pneumatically actuated transtibial prosthesis," *J. Bionic Eng.*, vol. 12, no. 2, pp. 217–226, Jun. 2015.

[21] H. Zheng, M. Wu, and X. Shen, "Variable series elasticity control of a pneumatically actuated transtibial prosthesis," *J. Med. Devices-Trans. Asme*, vol. 10, no. 3, Sep. 2016, Art. no. 030949.

[22] E. Garcia, J. C. Arevalo, G. Muñoz, and P. Gonzalez-De-Santos, "Combining series elastic actuation and magneto-rheological damping for the control of agile locomotion," *Robot. Auto. Syst.*, vol. 59, no. 10, pp. 827–839, Oct. 2011.

[23] E. J. Rouse, L. M. Mooney, and H. M. Herr, "Clutchable series-elastic actuator: Implications for prosthetic knee design," *Int. J. Robot. Res.*, vol. 33, no. 13, pp. 1611–1625, 2014.

[24] E. J. Rouse, L. M. Mooney, E. C. Martinez-Villalpando, and H. M. Herr, "Clutchable series-elastic actuator: Design of a robotic knee prosthesis for minimum energy consumption," in *Proc. IEEE Int. Conf. Rehabil. Robot.*, Jun. 2013, pp. 1–6.

[25] E. A. B. Nieto, S. Rezazadeh, and R. D. Gregg, "Minimizing energy consumption and peak power of series elastic actuators: A convex optimization framework for elastic element design," *IEEE-ASME Trans. Mechatronics*, vol. 24, no. 3, pp. 1334–1345, Jun. 2019.

[26] T. Verstraten, G. Mathijssen, R. Furnemont, B. Vanderborght, and D. Lefeber, "Modeling and design of geared DC motors for energy efficiency: Comparison between theory and experiments," *Mechatronics*, vol. 30, pp. 198–213, Sep. 2015.

[27] J. Bae, K. Kong, and M. Tomizuka, "Gait phase-based control for a rotary series elastic actuator assisting the knee joint," *J. Med. Devices*, vol. 5, no. 3, Sep. 2011, Art. no. 031010.

[28] K. Kong, J. Bae, and M. Tomizuka, "Control of rotary series elastic actuator for ideal force-mode actuation in human–robot interaction applications," *IEEE/ASME Trans. Mechatronics*, vol. 14, no. 1, pp. 105–118, Feb. 2009.

[29] T. Inaba, T. Nakazawa, and K. Koganezawa, "Stiffness and angle control of antagonistially driven joint using the actuator with non-linear elastic system (ANLES)," *J. Robot. Soc. Jpn.*, vol. 26, no. 4, pp. 381–388, May 2008.

[30] K. Koganezawa, T. Inaba, and T. Nakazawa, "Stiffness and angle control of antagonistially driven joint," in *Proc. IEEE/RAS-EMBS Int. Conf. Biomed. Robot. Biomechtron.*, Feb. 2006, pp. 1007–1013.

[31] S. A. Migliore, E. A. Brown, and S. P. Deweerth, "Biologically inspired joint stiffness control," in *Proc. IEEE Int. Conf. Robot. Autom.*, Apr. 2006, pp. 4508–4513.

[32] S. A. Migliore, E. A. Brown, and S. P. Deweerth, "Novel nonlinear elastic actuators for passively controlling robotic joint compliance," *J. Mech. Design*, vol. 129, no. 4, pp. 406–412, Apr. 2007.

[33] G. Tonietti, R. Schiavi, and A. Bicchi, "Design and control of a variable stiffness actuator for safe and fast physical human/robot interaction," in *Proc. IEEE Int. Conf. Robot. Autom.*, Apr. 2006, pp. 526–531.

[34] J. W. Hurst, J. E. Chestnutt, and A. A. Rizzi, "The actuator with mechanically adjustable series compliance," *IEEE Trans. Robot.*, vol. 26, no. 4, pp. 597–606, Aug. 2010.

[35] S. Lan and Z. Song, "Design of a new nonlinear stiffness compliant actuator and its error compensation method," *J. Robot.*, vol. 2016, Oct. 2016, Art. no. 1.
[36] J. W. Sensinger and R. F. Weir, "Design and analysis of a non-backdrivable series elastic actuator," in *Proc. 9th Int. Conf. Rehabil. Robot. (ICORR)*, Jun./Jul. 2005, pp. 390–393.
[37] J. W. Sensinger and R. F. Weir, "Non-backdrivable series elastic actuator for use in a prosthetic elbow," in *Proc. Myoelectric Controls Symp.*, Aug. 2005, pp. 67–70.
[38] F. Sergi and M. K. O'Malley, "On the stability and accuracy of high stiffness rendering in non-backdrivable actuators through series elasticity," *Mechatronics*, vol. 26, pp. 64–75, Mar. 2015.
[39] S. Wolf, O. Eiberger, and G. Hirzinger, "The DLR FSJ: Energy based design of a variable stiffness joint," in *Proc. IEEE Int. Conf. Robot. Autom.*, May 2011, pp. 5082–5089.
[40] G. Mathijssen, R. Furnemont, S. Beckers, T. Verstraten, D. Lefeber, and B. Vanderborght, "Cylindrical cam mechanism for unlimited subsequent spring recruitment in Series-Parallel Elastic Actuators," in *Proc. Int. Conf. Robot. Autom.*, May 2015, pp. 857–862.
[41] J. Realmuto, G. Klute, and S. Devasia, "Nonlinear passive cam-based springs for powered ankle prostheses," *J. Med. Devices*, vol. 9, no. 1, Mar. 2015, Art. no. 011007.
[42] F. Gao, Y. Liu, and W.-H. Liao, "Design of powered ankle-foot prosthesis with nonlinear parallel spring mechanism," *J. Mech. Des.*, vol. 140, no. 5, May 2018, Art. no. 055001.
[43] F. Gao, Y. Liu, and W.-H. Liao, "A new powered ankle-foot prosthesis with compact parallel spring mechanism," in *Proc. IEEE Int. Conf. Robot. Biomimetics (ROBIO)*, Dec. 2016, pp. 473–478.
[44] M. Liu, P. Datseris, and H. H. Huang, "A prototype for smart prosthetic legs-analysis and mechanical design," *Adv. Mater. Res.*, vols. 403–408, pp. 1999–2006, Nov. 2011.
[45] Y. Sun, W. Ge, J. Zheng, and D. Dong, "Design and evaluation of a prosthetic knee joint using the geared five-bar mechanism," *IEEE Trans. Neural Syst. Rehabil. Eng.*, vol. 23, no. 6, pp. 1031–1038, Nov. 2015.
[46] M. Grimmer and A. Seyfarth, "Mimicking human-like leg function in prosthetic limbs," in *Neuro-Robotics*, P. Artemiadis, Ed. Dordrecht, The Netherlands: Springer, 2014, pp. 105–155.
[47] E. Basafa, H. Salarieh, and A. Alasty, "Modeling and control of nonlinear series elastic actuator," in *Proc. ASME Int. Des. Eng. Tech. Conf. Comput. Inf. Eng. Conf.*, May 2007, pp. 127–133.
[48] D. W. Robinson, "Design and analysis of series elasticity in closed-loop actuator force control," Ph.D. dissertation, Dept. Mech. Eng., Massachusetts Inst. Technol., Cambridge, MA, USA, 2000.
[49] E. Bolívar, S. Rezazadeh, and R. Gregg, "A general framework for minimizing energy consumption of series elastic actuators with regeneration," in *Proc. ASME Dyn. Syst. Control Conf.*, Jan. 2017, p. V001T36A005. doi: 10.1115/DSCC2017-5373.
[50] Y. Sun, W. Ge, J. Zheng, F. Xia, and D. Dong, "Optimization of actuating torques in multi-bar prosthetic joints with springs," *Eng. Optim.*, vol. 49, no. 7, pp. 1183–1196, 2017.
[51] F. Gao, Y. Liu, and W. Liao, "Optimal design of a magnetorheological damper used in smart prosthetic knees," *Smart Mater. Struct.*, vol. 26, no. 3, Feb. 2017, Art. no. 035034.
[52] E. J. Rouse, L. J. Hargrove, E. J. Perreault, M. A. Peshkin, and T. A. Kuiken, "Development of a mechatronic platform and validation of methods for estimating ankle stiffness during the stance phase of walking," *J. Biomech. Eng.-Trans. ASME*, vol. 135, no. 8, Aug. 2013, Art. no. 081009.
[53] Y. Sun, W. Ge, J. Zheng, and D. Dong, "Solving the kinematics of the planar mechanism using data structures of assur groups," *J. Mech. Robot.*, vol. 8, no. 6, Dec. 2016, Art. no. 061002.

YUANXI SUN received the B.S. and Ph.D. degrees in mechanical engineering from Northwestern Polytechnical University, Xi'an, Shaanxi, China, in 2011 and 2017, respectively.

He is currently with the College of Mechanical Engineering, Chongqing University, Chongqing, China. His research interests include design, actuation and control of lower limb prosthesis, exoskeleton, and bionic robotics.

PEI TANG received the B.E. degree in mechanical engineering from the Chongqing University of Technology, Chongqing, China, in 2016. He is currently pursuing the M.E. degree in mechanical engineering with Chongqing University, Chongqing.

His current research interests include structure design and locomotion control of lower limb prosthesis.

JIA ZHENG received the B.S., M.S., and Ph.D. degrees in mechanical engineering from Northwestern Polytechnical University, Xi'an, China, in 2011, 2014, and 2019, respectively.

She is currently with the School of Advanced Manufacturing Engineering, Chongqing University of Posts and Telecommunications, Chongqing, China. Her research interests include neural networks, non-destructive detection, industrial computed tomography (CT)-based detection, and industrial CT image processing, with expertise in industrial CT image segmentation.

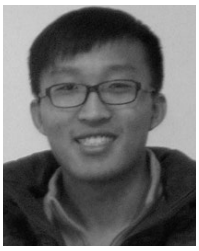

DIANBIAO DONG received the B.S. degree in mechanical engineering from Northwestern Polytechnical University, in 2013, where he is currently pursuing the Ph.D. degree. He has been a joint Ph.D. Student with the Department of Mechanical Engineering (MECH), Vrije Universiteit Brussel, since 2016.

His research interests include ankle-foot prosthetics and exoskeleton.

XIAOHONG CHEN received the B.S. and M.S. degrees in mechanical engineering from Northwestern Polytechnical University, Xi'an, China, in 2007 and 2011, respectively.

She is currently with the College of Mechanical Engineering, Chongqing University. Her research interests include bioinspired and biomimetic robotics, and lightweight lattice materials.

LONG BAI received the B.E., M.E., and Ph.D. degrees in mechanical engineering from Northwestern Polytechnical University, Xi'an, China, in 2005, 2008, and 2012, respectively.

He is currently an Associate Professor with the State Key Laboratory of Mechanical Transmission, and the College of Mechanical Engineering, Chongqing University, Chongqing, China. His research interests include bioinspired and biomimetic robotics, rehabilitated and surgical robotics, and lightweight lattice materials.

WENJIE GE received the B.S. degree in mechanical design and manufacturing from the Xi'an University of Technology, and the M.S. and Ph.D. degrees in mechanical engineering from Northwestern Polytechnical University.

He is currently a Professor with Northwestern Polytechnical University. His research interests include mechanical theory and mechanism, mechanical dynamics, robotic mechanism, and bionic robotics.